Single and double stage sintering of mechanically alloyed powder for nanostructured Ti6Al4V foams usable in cancellous scaffolds

S. K. Sadrnezhaad[1,2]*, M. Aryana[3,1], N. Hassanzadeh Nemati[3,1], M. Alizadeh[1] and A. Ebadifar[1,4]

Mechanical alloying and sintering were used to fabricate nanostructured Ti6Al4V scaffolds of highly controllable pore geometry and fully interconnected porous network. Elemental powders were milled for different periods of time (10, 20, 30, 40 and 60 h), mixed with 40–60 vol.-% of 200–400 μm cuboidal NaCl, compacted at 500–600 MPa and sintered according to single or double stage heat treatment regimes at 790 and 950°C under vacuum. After sintering, the samples were soaked in distilled water to washout the NaCl. Foamy microstructures were obtained showing well shaped biopores and fragmentary embedded micropores. The shape of initial NaCl was copied into the biopores which had highly interconnected architecture considered suitable for cancellous bone tissue adherence and cell culture.

Keywords: Biomimetic material, Dental alloy, Nanoparticle, Titanium alloy

Introduction

Titanium and its alloys possess low density, superior mechanical properties, good corrosion resistance and satisfactory biocompatibility. Although these characteristics are desirable for dental and orthopaedic implant manufacturing, substantial difference between their Young's modulus compared to that of hard tissue is a matter of concern. Stress shielding may, for example, cause trouble after their utilisation. Bone resorption and eventual implant loosening may also occur after their long term application.[1]

Interest in porous metallic scaffolds for bone tissue engineering has increased during recent years.[2] The porosity of foamy materials provides biological anchorage for penetration of hard tissues into the spongy structures[3] and allows long term fixation.[1] Foamy Ti6Al4V can mimic the biological and mechanical properties of the host bone.[4] There are several methods for fabrication of porous Ti6Al4V alloys including rapid prototyping,[5,6] powder metallurgy,[2,6] electron beam melting,[1] pore filled argon expansion[5] and space holder solid state foaming.[2] carbamide (urea),[7] ammonium hydrogen carbonate,[8] magnesium,[9] removable polymers[10,11] and sodium chloride have previously been used as space holders.[12,13]

Reduction of the scaffold density together with improvements in the mechanical properties is the major objective of this research. Foamy Ti6Al4V scaffolds are produced by a simple and direct method composed of mechanical alloying and subsequent compaction and sintering of the milled elemental powders. The procedure is straightforward and results in formation of foamy nanostructures having predefined pore sizes and required porosity percentages. Process parameters can be adjusted to obtain 100–400 μm pore dimensions. By choosing geometry, size distribution, quantity and appearance of the holders, the mechanical properties of the foamy product can be tuned to the biomedical applications range. Strength improvement due to lowering of the average crystallite size down to the nanoscale level is another benefit of the devised procedure which can facilitate nanostructure formation. Use of NaCl diminishes the production cost and simplifies the spacer removal from the milled products. The effects of the spacer fraction and the sintering stages on the foam structure are investigated.

Materials and methods

Prototype fabrication

The schematic drawing shown in Fig. 1 outlines processing steps used in this research. Spongy Ti and powders of Al and V were weighed out in the required proportions and mechanically alloyed together in a planetary ball mill (LG-IG5, SVO15IG5-1) with 2 wt-%

[1]Department of Metals, Institute of Materials Science and Engineering, Graduate University of Advanced Technology, Kerman, Iran
[2]Department of Materials Science and Engineering, Sharif University of Technology, Tehran, Iran
[3]Department of Biomedical Engineering, Science and Research Branch, Islamic Azad University, Tehran, Iran
[4]Dental Reseach Center of Shahid Beheshti University of Medical Sciences, Tehran, Iran

*Corresponding author, email sadrnezh@sharif.edu

Published by Maney on behalf of the Partnership
DOI 10.1179/1749514813Z.00000000052

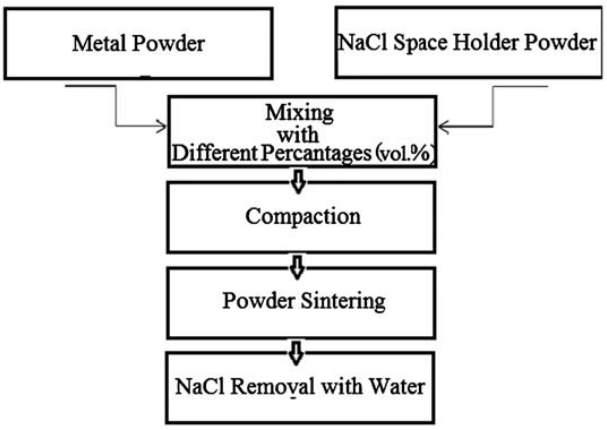

1 Schematic of stages for metallic foam fabrication

stearic acid addition. Specifications of the raw materials are listed in Table 1. Milling was carried out under protective atmosphere (99·998% purity Ar) with the milling parameters given in Table 2. Precise materials analyses showed no significant contamination of the powder mixture with environmental atmosphere or cup species even after long milling times.

Figure 2*a* shows an SEM image of the raw sodium chloride grains. Figure 2*b* is an SEM image of typical powder produced after 30 h milling of the elemental mixture. The milled powder was thoroughly mixed with different volume percentages of space holder and compressed into cylindrical green compacts by applying 600 MPa pressure. The green compacts were 10 mm diameter and 3 mm high. They were sintered under vacuum (10^{-5} torr) with a heating rate of 10°C min^{-1} at 790°C single stage (LTS), 950°C single stage (HTS) and 790°C followed by 950°C double-stage (LHTS) in an electric resistance furnace (HANYOUNG-PX9). Sintering time was 2 h for all stages. After the first sintering stage, all the samples were dipped into water for 48 h to remove the space holder. The second sintering stage was carried out after spacer removal. Figure 2*c–e* illustrates the microstructure of the salt removed foamy samples prepared according to LTS, HTS and LHTS procedures with 50 vol.-%NaCl.

Characterisation

Samples were taken for characterisation after milling for 10, 20 and 30 h. They were analyzed by X-ray diffractometer (Philips X'PERT MPD) using filtered Cu K_α radiation (λ=0·1542 nm). Archimedes' method was used for determination of the density and porosity of the sintered Ti6Al4V foams coated with a thin grease layer:

$$\Omega = \frac{M_2 - M_1}{M_2 - M_3} \quad (1)$$

where Ω is porosity, M_2 is weight of the sample in atmosphere (dry but pores filled with distilled water), M_1 is weight of the sample in atmosphere (full dry: pores without any water) and M_3 is weight of the sample while sunk in distilled water. Microscopic analyses of the samples were obtained by SEM (Philips XL30) equipped with energy dispersive X-ray analyser.

Results and discussion

The effect of NaCl on the foams produced via HTS and LHTS is illustrated in Fig. 2 with SEM images. It is seen that both sintering temperature and spacer quantity affect on pore architecture and hence mechanical properties of the samples produced as illustrated in the literature.[4] Both large (200–500 μm) and small (<10 μm) pores are observed in Fig. 2*e*. The former shows the geometry of the removed spacer grains, but the latter is caused by incomplete sintering at the first sintering stage. Second stage sintering under high vacuum (10^{-5} torr) results in strong bonding of grains and diminution of the small pore percentage.

The LTS procedure gives a pore geometry similar to the space holder shape (Fig. 2*c*). Pore coalescence is observed in samples sintered at 790°C with typical appearance as highlighted in Fig. 2*c* and *e*. Increasing the sintering temperature strengthens sample structure, improves densification and minimises spacer shape replication due to melting of the NaCl (Fig. 2*d*). Second stage sintering at 950°C (procedure LHTS), however, preserves the shape inherited from the first sintering stage and densifies the network structure (Fig. 2*e*).

Figure 3 shows the XRD patterns of the mixture after ball milling for 10, 20 and 30 h and the foam fabricated from 30 h milled Ti6l4V powder after two-stage LHTS sintering procedure. Both peak broadening and reduction in peak intensities are observed after milling for 20 h. Further milling up to 30 h results in excessive peak broadening and reduction of α(002) and β(110) peak sharpness. These changes show particle size diminution down to the nanometre scale which is consistent with peak change interpretations of Williamson and Hall.[14] Because of high activity of Ti, it is prone to oxygen adsorption, especially at high temperatures. Titanium oxide peaks are observable in XRD pattern of the sintered samples (Fig. 3*d*).

Table 2 Milling parameters

Ball mill machine	Planetary
Rotation speed of cup/rev min^{-1}	200
Cup material	Steel
Cup capacity/mL	150
Ball material	Steel
Diameter of balls/mm	15, 20
Number of balls	7
Balls to powders ratio	10 : 1
Total powders mass/g	20

Table 1 Specifications of raw materials

Material	Purity	Particle size	Particle shape	Supplier
Sponge Ti	99·9%	3–8 mm	Irregular	Alfa Aesar
Al powder	99%	45 μm	Irregular	Riedel-de Haen Germany
V powder	99%	5 μm	Irregular	Riedel-de Haen Germany
NaCl powder	99%	0·2–0·4 mm	Cuboidal	Merck

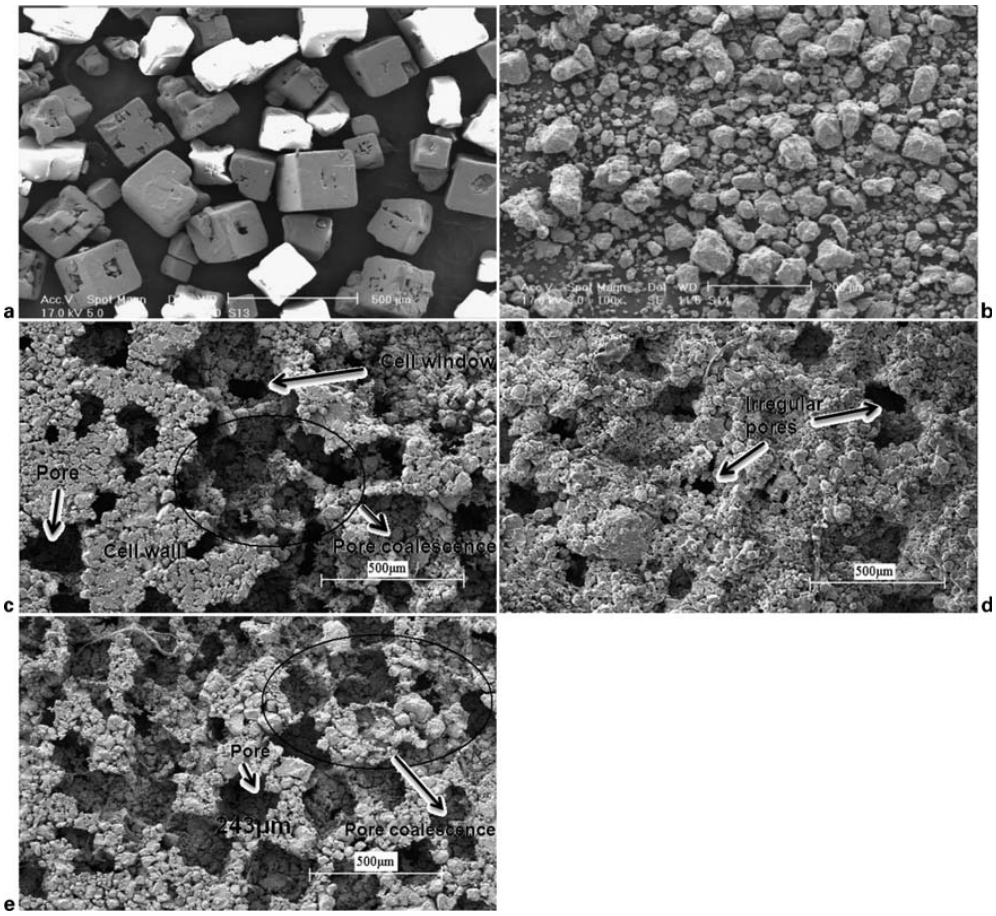

2 Images (SEM) of *a* sodium chloride raw material, *b* Ti, Al and V metallic elements milled for 30 h, then sintered at *c* 790°C, *d* 950°C and *e* first at 790°C and then at 950°C: after first sintering stage, NaCl (50 vol.-%) was removed by water

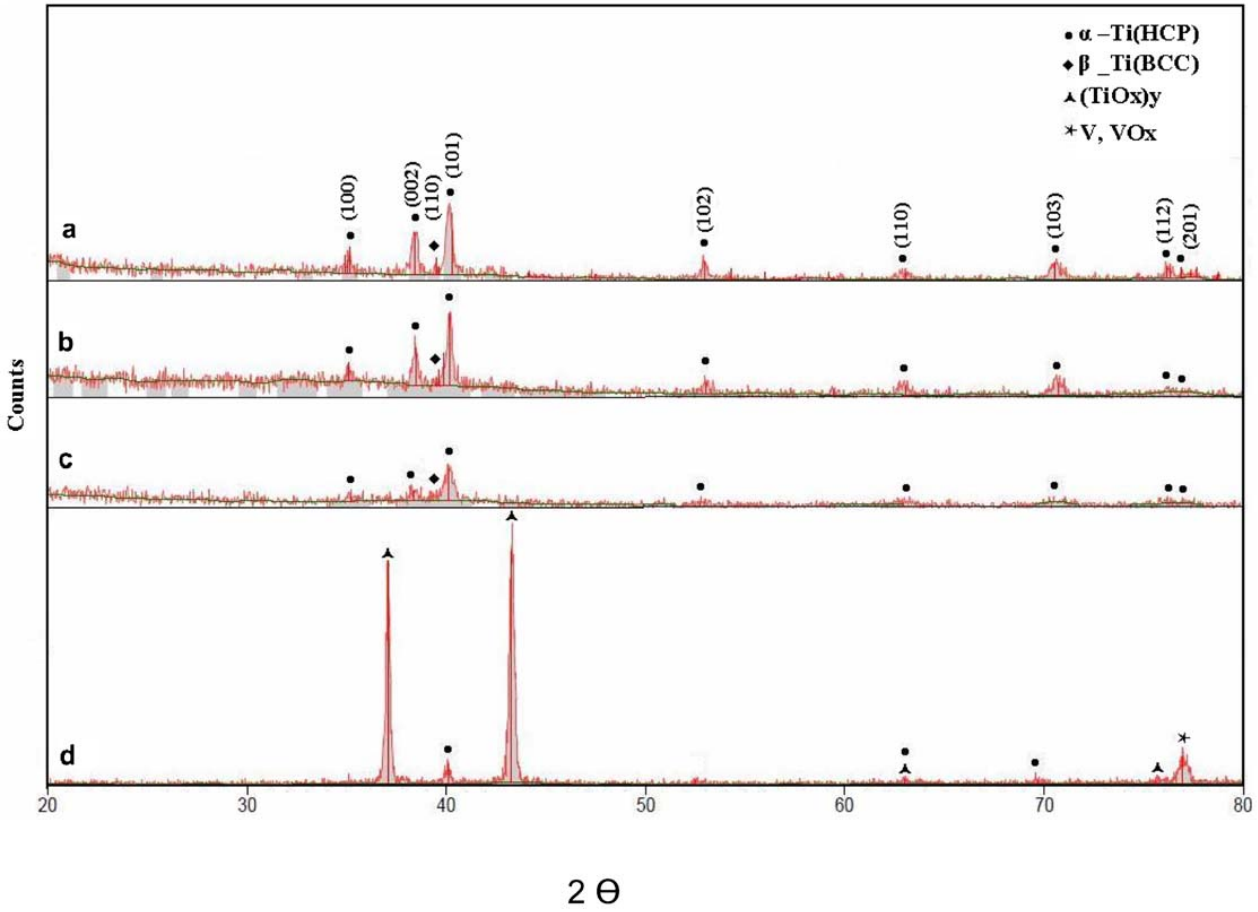

3 XRD patterns of pure Ti, Al and V mixture after ball milling for *a* 10, *b* 20 and *c* 30 h and *d* 30 h plus LHTS sintering procedure

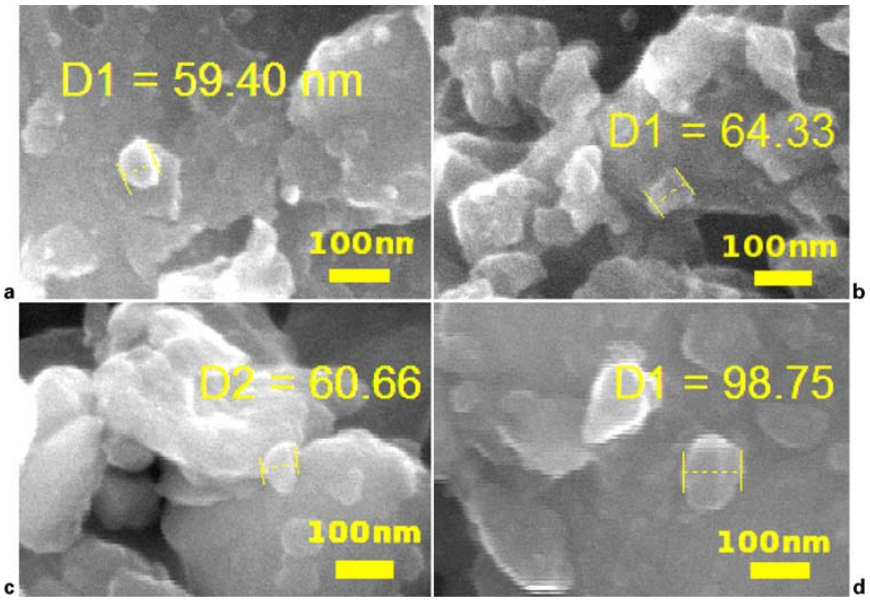

4 Nanosize crystallites highlighted in SEM images of samples after *a* 20, *b* 30, *c* 40 and *d* 60 h milling

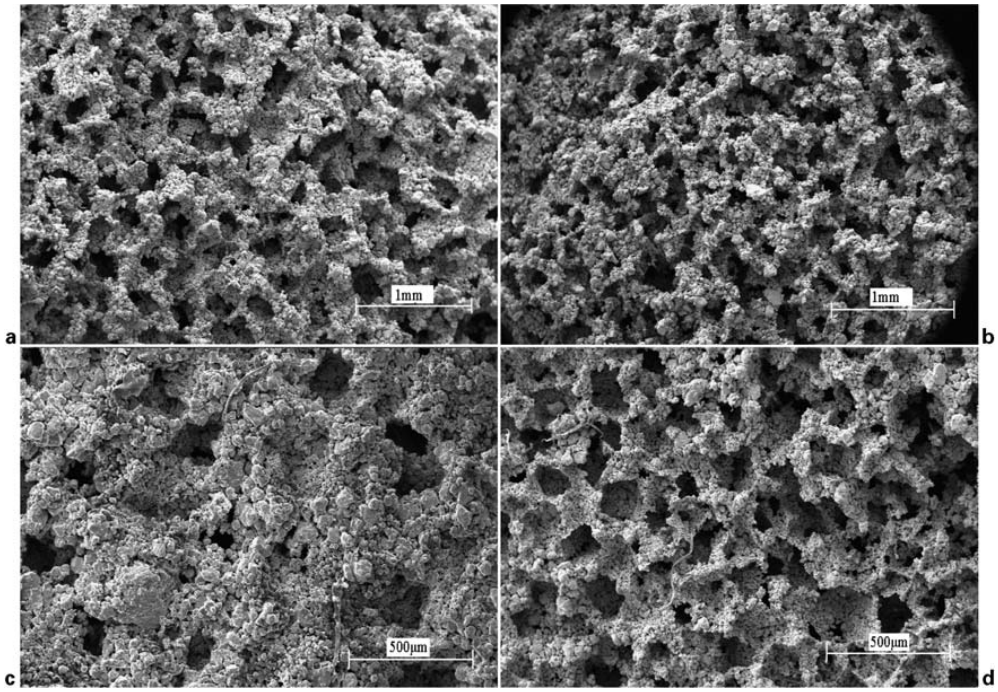

5 Scanning electron micrographs of Ti6Al4V foam produced according to procedure LHTS with *a* 70 and *b* 80 vol.-%NaCl and HTS with *c* 40 and *d* 50 vol.-%NaCl

The sizes of the Ti α(101) and β(110) peaks decline; however, because of Ti alloying during both milling and sintering treatments. Crystallite size and lattice strain of the powders after milling are evaluated by using Williamson–Hall and Scherer equations. The results are given in Table 3. As is expected, the data of Table 3 indicate lower crystallites sizes concomitant with higher lattice strains. The initial size enhancement at $10<t\leq20$ h can be attributed to the double (or multi-) particle welding at initial stages of milling. Subsequent brittle–ductile interactions at $20<t\leq30$ h can result in steep lowering of the crystallites size at longer milling times. SEM images of the samples milled for 20, 30, 40 and 60 h are shown in Fig. 4. Formation of nanoparticles after milling is clearly observable from the figure. Because of partial clustering of the grains, the apparent crystallite sizes obtained from these illustrations are slightly bigger than the data calculated from XRD peaks according to the Bragg law of diffraction evaluations. However, their average diameter fits within

Table 3 Crystallite size and lattice strain versus milling duration of samples

Milling time/h	Crystallite size/nm	Lattice strain/%
10	30·8	0·328
20	35·8	0·282
30	12·6	0·801

Table 4 EDS analyses of samples produced

Sintering procedure	Sintering temperaure/°C	Space holder/vol.-%	Component/at.%		
			Ti	Al	V
LTS	790	40	92·88	2·87	3·87
		50	91·96	2·22	4·41
HTS	950	40	88·41	5·93	4·87
		50	89·47	4·11	5·56
		60	91·69	3·76	4·42
LHTS	First stage: 790	40	92·22	0·52	7·26
	Second stage: 950	50	90·00	3·98	6·01
		60	93·49	1·46	4·79

Table 5 Standard and actual vapour pressures of foam constituents at sintering temperatures calculated from data of reference[16] by assumption of ideal behaviour for foam constituents

Sintering temperature/°C	Vapour Pressure/Pa				
	Al	Ti	V	$\frac{P^{o}_{Al}}{P^{o}_{Ti}}$	$\frac{P^{v}_{Al}}{P^{v}_{Ti}}$
790	0·1274	0·0002	0·0000	637	19·7
950	0·9000	0·0040	0·0008	225	15·1

Table 6 Effect of sintering regimes on density and porosity of foamy samples

Sintering procedure	Sintering temperature/°C	NaCl/%	Density/g cm^{-3}	Porosity/vol.-%
LHTS	First stage: 790	40	2·73	37·3
	Second stage: 950	50	2·53	39·6
HTS	950	40	2·05	49·3
		50	1·94	50·7

the nanometre scale and indicates approximate rise of the mean crystallite size at initial milling stage. Further size lowering was observed at longer milling durations.

Microscopic observations indicated formation of interconnected open pores in the samples made with 50 vol.-%NaCl. Highly porous samples are prone to crack propagation which increases their brittleness and reduces their impact energy absorption.[15] From previous literature,[1] it is inferable, however, that the highly interconnected pore structures produced with 80 and 50 vol.-%NaCl according to LHTS and HTS procedures of Fig. 5*b* and *d* are desirable for bone tissue engineering applications. Highly controllable geometry of the pores by LHTS procedure is clearly a major advantage for eventual optimum selection of the procedure.

EDS results reported in Table 4 indicate that with the same amount of NaCl, the Al contents of the foam after all LTS, HTS and LHTS procedures are lower than the aimed 6 at-%. Vapour pressures summarised in Table 5 indicate significant vaporisation of Al especially at high temperatures. Ti vaporisation is lower than Al and that of V is negligible. Although the actual vapour pressures of the substances given in Table 5[16] may differ due to non-ideal behaviour, the differences are so big that the effect of non-ideality does not change the trend.

While LTS and LHTS sintering at 790°C preserves almost all Ti content, HTS sintering at 950°C shows Ti reduction with respect to the aimed 90% due to much higher Ti vapour pressure. Longer exposure times of the LHTS samples to high temperature vacuum conditions result in larger Al vaporisation. Vaporisation loss can, of course, be compensated for by larger additions in the original mix. The data in Table 4 also show the protective effect of higher NaCl percentage on Ti loss. Oxygen adsorption at 790°C results in thin TiO_2 film formation and partial foam passivation in the second sintering stage of LHTS samples. Ti content in the LTS samples is thus higher than LHTS and HTS samples, as seen in Table 4. Longer exposure time of the lateral surfaces during the first stage sintering seems to be causing this effect.

Density and porosity of the LHTS and HTS samples made with 40 and 50 vol.-%NaCl are shown in Table 6. Density decrease and porosity increase with NaCl addition are observed. Experimental observations show that because of insufficient joining of the powder grains at 790°C, some particles are easily detached from the LTS samples. Detachment of the particles is not as easy in the HTS and LHTS samples, however.

Conclusions

Nanostructured Ti6AI4V foam was produced by milling of the elemental powders, compaction and sintering of the milled product with NaCl and salt removal with distilled water. Full retainment of sample architecture throughout the fabrication process and elimination of NaCl was observed. Microstructural observations indicated the formation of interconnected open cells in the samples made with 50 vol.-%NaCl. Morphological studies indicated 200–400 μm average pore diameters of these samples. Sintering resulted in pore coalescence at 790°C and drastic shape change at 950°C. Two-stage sintering resulted in NaCl shape replication together with pore network configuration.

Acknowledgements

Financial support of International Center for Science, High Technology & Environmental Sciences, Kerman, Iran (contract No. 1·78) is appreciated.

References

1. X. Li, C. Wang, W. Zhang and Y. Li: *Mater. Lett.*, 2009, **63**, 403.
2. G. Ryan, A. Pandit and D. P. Apatsidis: *Biomaterials*, 2006, **27**, 2651.
3. V. Karageorgiou and D. Kaplan: *Biomaterials*, 2005, **26**, (27), 5474.
4. A. Bandyopadhyay, F. Espana, V. K. Balla, S. Bose, Y. Ohgami and N. M. Davies: *Acta Biomater.*, 2010, **6**, (4), 1640.
5. G. E. Ryan, A. S. Pandit and D. P. Apatsidis, *Biomaterials*, 2008, **29**, 3625.
6. J. P. Lia, J. P. de Wijna, C. A. van Blitterswijka and K. de Groot, *Biomaterials*, 2006, **27**, 1223.
7. N. G. Davis, J. Teisen, C. Schuh and D. C. Dunand: *J. Mater. Res.*, 2001, **16**, (5), 1508.
8. M. Bram: *Adv. Eng. Mater.*, 2000, **2**, 196.
9. C. E. Wen, M. Mabuchi, Y. Yamanda, K. Shimojima, Y. Chino and T. Asahina: *Scr. Mater.*, 2001, **45**, 1147.
10. Z. Esen and S. Bor: *Scr. Mater.*, 2007, **56**, 341.
11. C. Jee, Z. Guo, J. Evans and N. Ozguven: *Metall. Mater. Trans. B*, 2000, **31B**, 1345.
12. Y. Orlova, K. Maekawal and H. J. Rack: in 'Recent developments in processing/applications of structural alloys, (ed. S. Spigarelli and M. Cabibbo), 411; 2009, Stafa/Zurich, Trans. Tech. Publications Ltd.
13. A. Manonukul, N. Muenya, F. Leaux and S. Amaranan: *J. Mater. Process. Technol.* 2010, **210**, 529.
14. G. K. Williamson and W. H. Hall: *Acta Metall.*, 1953, **1**, 22.
15. P. Siegkas, V. L. Tagarielli, N. Petrinic and L. P. Lefebvre: *J. Mater. Sci.*, 2011, **46**, 2746.
16. O. Kubaschewski, C. B. Alcock and P. S. Spencer: 'Materials thermochemistry', 6th edn; 1993, New York, Pergamon Press.